

on the model applied (particularly on the assumed degree of metal-silicate equilibration during core formation), resulting in age estimates ranging from ~30 to >100 My after solar system formation (20–22). In contrast, the Hf-W age of LMO crystallization tightly constrains the age of the Moon and the final stage of Earth's accretion to 30 to 50 My after the formation of the solar system. The formation of the Moon significantly later than that of asteroids and Mars (18, 27) underpins the Moon's origin by a unique event, as required in the giant impact hypothesis.

References and Notes

1. R. M. Canup, E. Asphaug, *Nature* **412**, 708 (2001).
2. R. W. Carlson, G. W. Lugmair, *Earth Planet. Sci. Lett.* **90**, 119 (1988).
3. C. Alibert, M. D. Norman, M. T. McCulloch, *Geochim. Cosmochim. Acta* **58**, 2921 (1994).
4. L. E. Borg et al., *Geochim. Cosmochim. Acta* **63**, 2679 (1999).
5. D.-C. Lee, A. N. Halliday, G. A. Snyder, L. A. Taylor, *Science* **278**, 1098 (1997).
6. J. H. Jones, H. Palme, in *Origin of the Earth and Moon*, R. M. Canup, K. Righter, Eds. (Univ. Arizona Press, Tucson, AZ, 2000), pp. 197–216.

7. C. K. Shearer, H. E. Newsom, *Geochim. Cosmochim. Acta* **64**, 3599 (2000).
8. I. Leya, R. Wieler, A. N. Halliday, *Earth Planet. Sci. Lett.* **175**, 1 (2000).
9. D. C. Lee, A. N. Halliday, I. Leya, R. Wieler, U. Wiechert, *Earth Planet. Sci. Lett.* **198**, 267 (2002).
10. H. Wänke et al., *Proc. Sec. Lunar Planet. Sci. Conf.* **2**, 1187 (1971).
11. C. K. Shearer, J. J. Papike, *Am. Mineral.* **84**, 1469 (1999).
12. P. H. Warren, J. T. Wasson, *Rev. Geophys. Space Phys.* **17**, 73 (1979).
13. H. Palme, H. Wänke, *Proc. Lunar Sci. Conf.* **6**, 1179 (1975).
14. K. Righter, C. K. Shearer, *Geochim. Cosmochim. Acta* **67**, 2497 (2003).
15. I. Leya, R. Wieler, A. N. Halliday, *Geochim. Cosmochim. Acta* **67**, 529 (2003).
16. L. E. Nyquist et al., *Geochim. Cosmochim. Acta* **59**, 2817 (1995).
17. H. Palme, W. Rammensee, *Lunar Planet. Sci.* **XII**, 796 (1981).
18. T. Kleine, C. Münker, K. Mezger, H. Palme, *Nature* **418**, 952 (2002).
19. Q. Z. Yin et al., *Nature* **418**, 949 (2002).
20. S. B. Jacobsen, *Annu. Rev. Earth Planet. Sci. Lett.* **33**, 531 (2005).
21. A. N. Halliday, *Nature* **427**, 505 (2004).
22. T. Kleine, K. Mezger, H. Palme, E. Scherer, C. Münker, *Earth Planet. Sci. Lett.* **228**, 109 (2004).
23. L. T. Elkins-Tanton, J. A. Van Orman, B. H. Hager, T. L. Grove, *Earth Planet. Sci. Lett.* **196**, 239 (2002).

24. S. C. Solomon, J. Longhi, *Proc. Lunar Sci. Conf.* **8**, 583 (1977).
25. H. Palme, *Geochim. Cosmochim. Acta* **41**, 1791 (1977).
26. R. W. Carlson, G. W. Lugmair, *Earth Planet. Sci. Lett.* **45**, 123 (1979).
27. T. Kleine, K. Mezger, H. Palme, E. Scherer, C. Münker, *Geochim. Cosmochim. Acta*, in press.
28. T. Kleine, K. Mezger, C. Münker, H. Palme, A. Bischoff, *Geochim. Cosmochim. Acta* **68**, 2935 (2004).
29. T. Kleine, K. Mezger, H. Palme, E. Scherer, C. Münker, *Earth Planet. Sci. Lett.* **231**, 41 (2005).
30. We thank NASA for providing the samples for this study and I. Leya, R. Wieler, L. Borg, T. Grove, T. Irving, S. Jacobsen, L. Nyquist, and two anonymous reviewers for their comments. E. Scherer supported the MC-ICPMS in Münster, and C. Münker provided aliquots of the whole-rock samples. This study was supported by the Deutsche Forschungsgemeinschaft as part of the research priority program "Mars and the terrestrial planets" and by a European Union Marie Curie postdoctoral fellowship to T.K.

Supporting Online Material

www.sciencemag.org/cgi/content/full/310/5754/1671/DC1  
 SOM Text  
 Tables S1 and S2  
 References

15 August 2005; accepted 10 November 2005  
 10.1126/science.1118842

# The Importance of Land-Cover Change in Simulating Future Climates

Johannes J. Feddema,<sup>1\*</sup> Keith W. Oleson,<sup>2</sup> Gordon B. Bonan,<sup>2</sup> Linda O. Mearns,<sup>2</sup> Lawrence E. Buja,<sup>2</sup> Gerald A. Meehl,<sup>2</sup> Warren M. Washington<sup>2</sup>

Adding the effects of changes in land cover to the A2 and B1 transient climate simulations described in the Special Report on Emissions Scenarios (SRES) by the Intergovernmental Panel on Climate Change leads to significantly different regional climates in 2100 as compared with climates resulting from atmospheric SRES forcings alone. Agricultural expansion in the A2 scenario results in significant additional warming over the Amazon and cooling of the upper air column and nearby oceans. These and other influences on the Hadley and monsoon circulations affect extratropical climates. Agricultural expansion in the mid-latitudes produces cooling and decreases in the mean daily temperature range over many areas. The A2 scenario results in more significant change, often of opposite sign, than does the B1 scenario.

As anthropogenic impacts on Earth's surface continue to accelerate, the effects of these actions on future climate are still far from known (1–3). Historical land-cover conversion by humans may have decreased temperatures by 1° to 2°C in mid-latitude agricultural regions (4–9). Simulations of tropical deforestation (10–12) and potential future human land-cover impacts project a warming of 1° to 2°C in deforested areas (13, 14), with possible ex-

tratropical impacts due to teleconnection processes (7, 11, 13, 15). However, most of these experiments have been performed in uncoupled or intermediate-complexity climate models and have not followed the proposed framework of the Intergovernmental Panel on Climate Change (IPCC) Special Report on Emissions Scenarios (SRES) (16). The study described here evaluated whether future land use decisions, based on assumptions similar to those used to create the IPCC SRES atmospheric forcing scenarios, could alter the outcomes of two future IPCC SRES climate simulations.

Land-cover impacts on global climate can be divided into two major categories: biogeochemical and biogeophysical (2, 14–18).

Biogeochemical processes affect climate by altering the rate of biogeochemical cycles, thereby changing the chemical composition of the atmosphere. To some extent, these emissions are included in the IPCC climate change assessments (1). Biogeophysical processes directly affect the physical parameters that determine the absorption and disposition of energy at Earth's surface. Albedo, or the reflective properties of Earth's surface, alters the absorption rate of solar radiation and hence energy availability at Earth's surface (4–19). Surface hydrology and vegetation transpiration characteristics affect how energy received by the surface is partitioned into latent and sensible heat fluxes (4–19). Vegetation structure affects surface roughness, thereby altering momentum and heat transport (12). Summarizing the effects of land-cover change on climate has been difficult because different biogeophysical effects offset each other in terms of climate impacts (16), and, on global and annual scales, regional impacts are often of opposite sign and are therefore not well represented in annual global average statistics (7, 16).

For this study, we used the fully coupled Department of Energy Parallel Climate Model (DOE-PCM) (20, 21) to simulate combined land-cover and atmospheric forcings for the A2 and B1 IPCC SRES scenarios (22). Atmospheric forcings were identical to those used in previous IPCC SRES scenario experiments, resulting in a 1°C warming for the low-impact B1 scenario and a 2°C warming for the high-impact A2 scenario (20). To simulate future land-cover change, we used the Integrated Model to Assess the Global Environment (IMAGE) 2.2 IPCC SRES land-cover projections (7, 22–24) and DOE-PCM natural vegetation data to create land-cover data sets

<sup>1</sup>Department of Geography, University of Kansas, Lawrence, KS 66045, USA. <sup>2</sup>National Center for Atmospheric Research, Post Office Box 3000, Boulder, CO 80307, USA.

\*To whom correspondence should be addressed. E-mail: feddema@ku.edu

representing SRES B1 and A2 scenarios for the years 2050 and 2100 (Fig. 1) [for further details, see section A of the Supporting Online Material (25)]. For each SRES scenario, we ran the model from 2000 to 2033 with present-day land cover, from 2033 to 2066 with 2050 land cover, and from 2066 to 2100 with 2100 land cover. The model ran in transient mode, using IPCC atmospheric forcings from 2000 to 2100 (20). For comparison, we ran the same simulations with identical IPCC SRES atmospheric forcing while holding land cover constant at the present-day conditions (Fig. 1). To isolate the effects produced by land-cover change, results are presented as the difference between the all-forcing scenario (atmospheric and land-cover) and the atmospheric forcing with constant land cover. To illustrate the robustness of our results, we conducted a

second A2 scenario simulation that held land cover constant at present conditions to 2066 and then switched to the A2 2100 land-cover scenario [for further details, see section B of the Supporting Online Material (25)]. This experiment showed almost identical results, with similar statistical significance, as the initial A2 2100 experiment (fig. S1).

Land-cover change effects on global surface temperatures differ significantly between the A2 and B1 climate scenarios (Fig. 2). However, globally averaged annual temperature differences for a given scenario are less than 0.1°C for all the simulations because of offsetting regional climate signals. Most significant regional climate effects are associated directly with land-cover conversions in mid-latitude and tropical areas. At higher latitudes, temperature responses are not directly linked

to local land-cover change and can change sign by season (Fig. 2). Compared to surface temperature responses, land-cover change has a more significant effect on diurnal temperature ranges (DTRs) (Fig. 3). All scenarios show widespread DTR responses to land-cover change, and many of the changes correspond directly with areas of land-cover change. In three of the four scenarios, the DTR decreases significantly in southern Asia; and in the A2 scenarios, significant portions of the mid-latitude land areas experience decreases in DTRs. To better understand the potential effects and mechanisms of the impacts of land-cover change, six regions have been selected to illustrate the nature of the response (Fig. 1).

In the Amazon, the direct effect of converting tropical broadleaf forest to agriculture in the A2 2100 scenario is a significant warm-

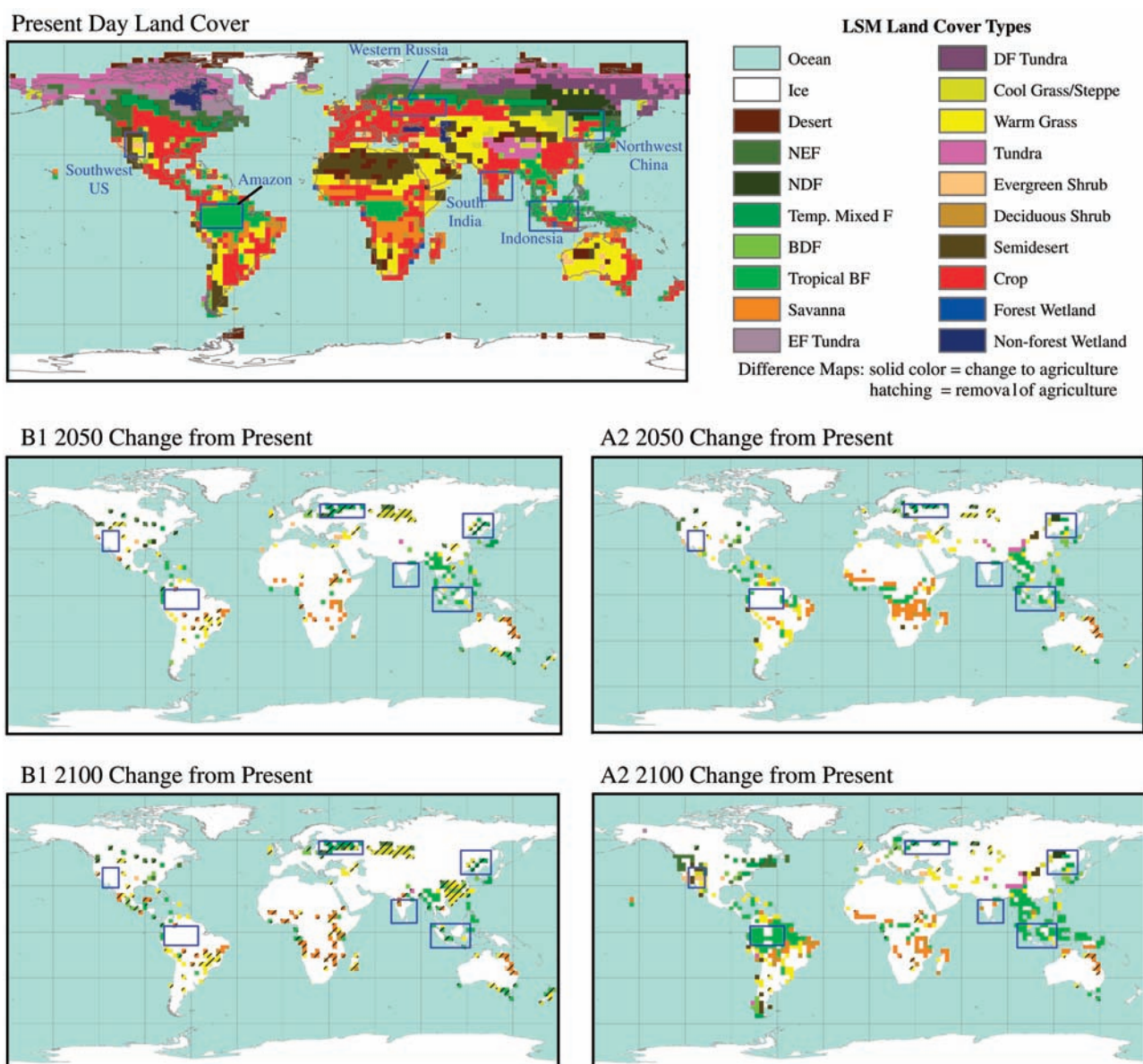


**Fig. 1.** Representation of present-day land cover and land-cover change for each of the scenarios. Each of the six tropical regions discussed in the text is indicated. B, broadleaf; N, needleleaf; E, evergreen; D, deciduous; and F, forest.

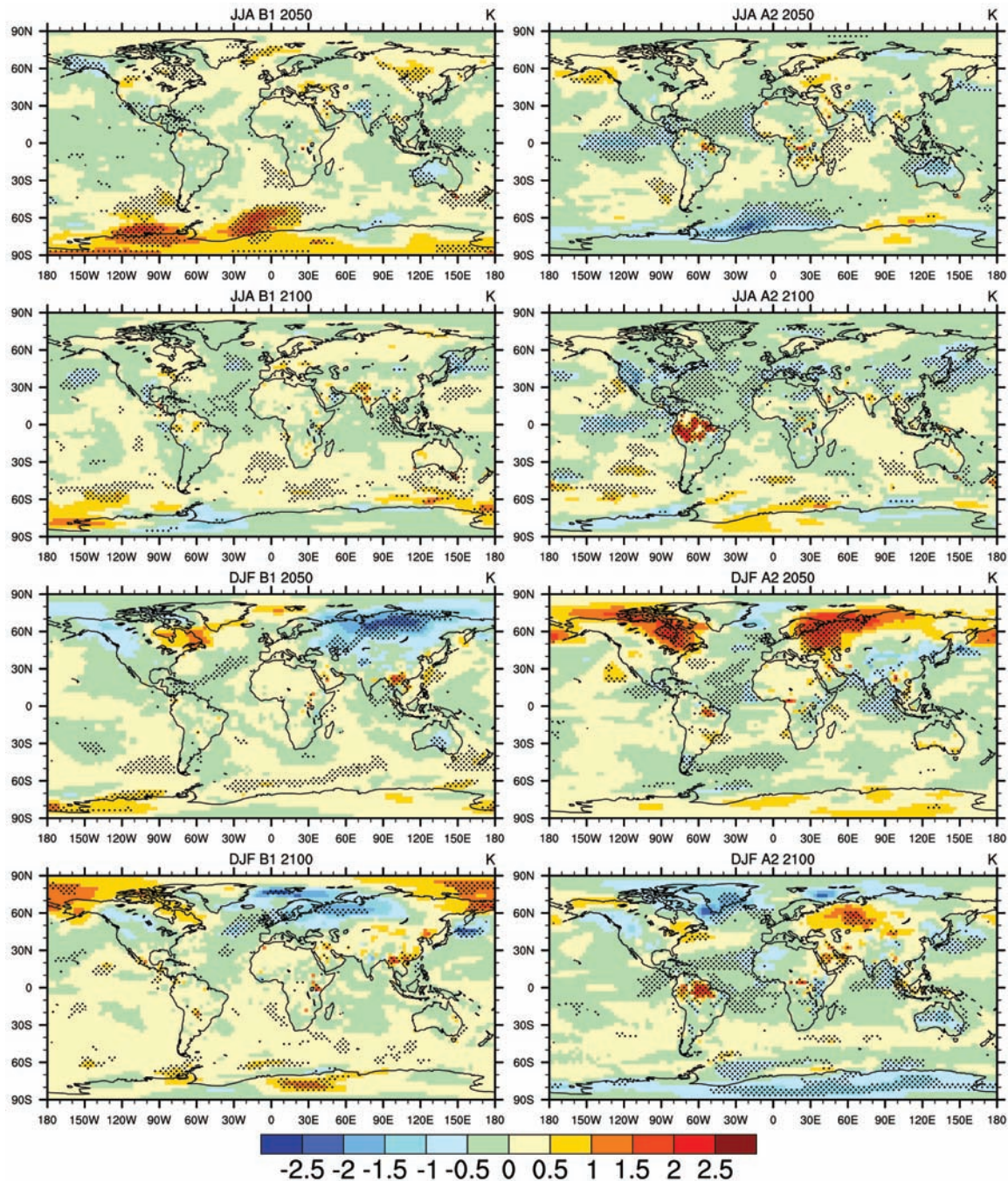
ing, well above 2°C (Fig. 2). However, the same land-cover conversion results in relatively minor temperature responses in Indonesia. From these observations, it is apparent that tropical locations with the same land-cover forcing have different responses, as has been shown in other studies (12, 13). To assess these different regional responses, we evaluated temperature responses in all grid cells that were converted from tropical broadleaf evergreen forest to agriculture [for further details, see section C of the Supporting Online Material (25)]. In almost all cases, this land-cover change has minor effects on daily maximum temperatures. However, in the Amazon there is

a significant increase in daily minimum temperatures, an effect not observed in Indonesia (fig. S2). The changes in minimum temperatures are most often associated with dry periods [for further details, see section C of the Supporting Online Material (25)]. Therefore, it is primarily the increase in daily minimum temperatures, typically at nighttime, that affects the DTR in tropical regions. Increased nighttime temperatures are known to cause a disproportionate human stress response (26).

Further analysis of the tropical regions shows that in the Amazon, net radiation changes in the atmospheric forcing scenarios are primarily offset by increases in latent heat

fluxes when tropical forests are present. These increases in latent heat fluxes increase cloud cover and minimize temperature impacts. In comparable land-cover and atmospheric forcing simulations, the lower leaf-area index over the region reduces latent heat flux and cloud cover, resulting in increased incident radiation. These processes increase surface temperatures and sensible heat flux. In the present-day and A2 atmospheric forcing scenarios, moisture fluxes from canopy evaporation, ground evaporation, and transpiration are partitioned as 22, 20, and 58%, respectively. When the A2 2100 land-cover change is included, this changes to 10, 63, and 26%. In contrast, In-

**Fig. 2.** JJA and DJF temperature differences due to land-cover change in each of the scenarios. Values were calculated by subtracting the greenhouse gas-only forcing scenarios from a simulation including land-cover and greenhouse gas forcings. Shaded grid cells are significant at the 0.05 confidence level. The top four panels show JJA; the bottom four show DJF. B1 scenario results are on the left and A2 results are on the right.



onesia does not experience a reduction in latent heat flux even though there is a 20% reduction in the fraction of latent heat flux that is transpired. In this case, an increase in local rainfall provides water to increase evaporation rates, thereby compensating for increases in sensible heat flux and temperature. The lack of response over Indonesia can be attributed to the effects of the Asian Monsoon circulation and precipitation regime, which override feedbacks from local land-cover change.

Although the Asian Monsoon suppresses the Indonesian response to land-cover forcing, other large-scale land-cover forcings in East Africa, Australia, and southern and eastern Asia appear to affect the strength and timing of the large-scale Asian Monsoon circulation. This results in climate impacts over a number of areas that are influenced by the Asian Monsoon. For example, both 2050 scenarios over India in June, July, and August (JJA) show increased cloud cover and precipitation, resulting in decreased incident radiation and higher latent heat fluxes. This effect occurs despite local reductions in transpiration efficiencies due to local land-cover change. This reverses in the A2 2100 scenario, perhaps because the effect of African land-cover change on the monsoon circulation is reduced. The B1 2100 scenario, with global reforestation, results in significantly dryer and warmer Indian climates. Similar impacts occur in East

Africa and northern Australia. Temperatures over the Indian Ocean are also affected, with possible consequences for the North Atlantic Oscillation (27).

Compared to Asia, Amazonian land-cover feedbacks have much greater local impacts. Although surface temperatures increase dramatically in response to land-cover forcing, temperatures in the air column above show a significant cooling as compared to the atmospheric forcing scenario. This slows the regional Hadley circulation and has significant impacts over nearby ocean areas. The Atlantic Ocean experiences a significant cooling that extends from the tropical warm pool to much of the North Atlantic in the A2 2100 JJA scenario. The eastern equatorial Pacific also shows a significant cooling response in the A2 scenario, suggesting more La Niña-like conditions. In the B1 scenario, a slight cooling in the western equatorial Pacific Ocean in 2050 and slight warming over the eastern Pacific Ocean in 2100 suggest a more El Niño-like state.

The impacts of land-cover change on extratropical climates are in response to a mixture of local land-cover change effects and changes in the large-scale circulation system. The conversion of mid-latitude forests and grasslands to agriculture is generally thought to cool mean daily maximum temperatures (28, 29). This direct land-cover effect is evident in northeast China, where the conver-

sion to agriculture results in relative cooling (or reduced warming in the all-forcing scenario) and decreased DTR due to increases in winter albedo and summer evapotranspiration efficiencies. This contrasts strongly with the warming, also in southern China, in the B1 scenario when existing agricultural areas are replaced with forest.

In the A2 2100 scenario, a less direct response to land cover is observed in the southwestern United States. There, transpiration efficiencies increase significantly with local land conversion to agriculture. But increased latent heat fluxes are only realized because of a significant increase in local precipitation, a result that is opposite to that found in similar uncoupled studies (15). In this case, the weakened Hadley circulation, caused by Amazon deforestation and cooler temperatures over the neighboring ocean areas, allows a greater northward migration of the Intertropical Convergence Zone (ITCZ) and more moisture entrainment to intensify southwest monsoon precipitation in summer. The increase in latent heat flux, from increased water availability and transpiration efficiency, results in the cooling of mean daily maximum temperatures. The same process also explains the cooling over the eastern Pacific and western Atlantic Oceans, where increased cloud cover and precipitation associated with an expanded northward migration of the ITCZ result in cooler temperatures.

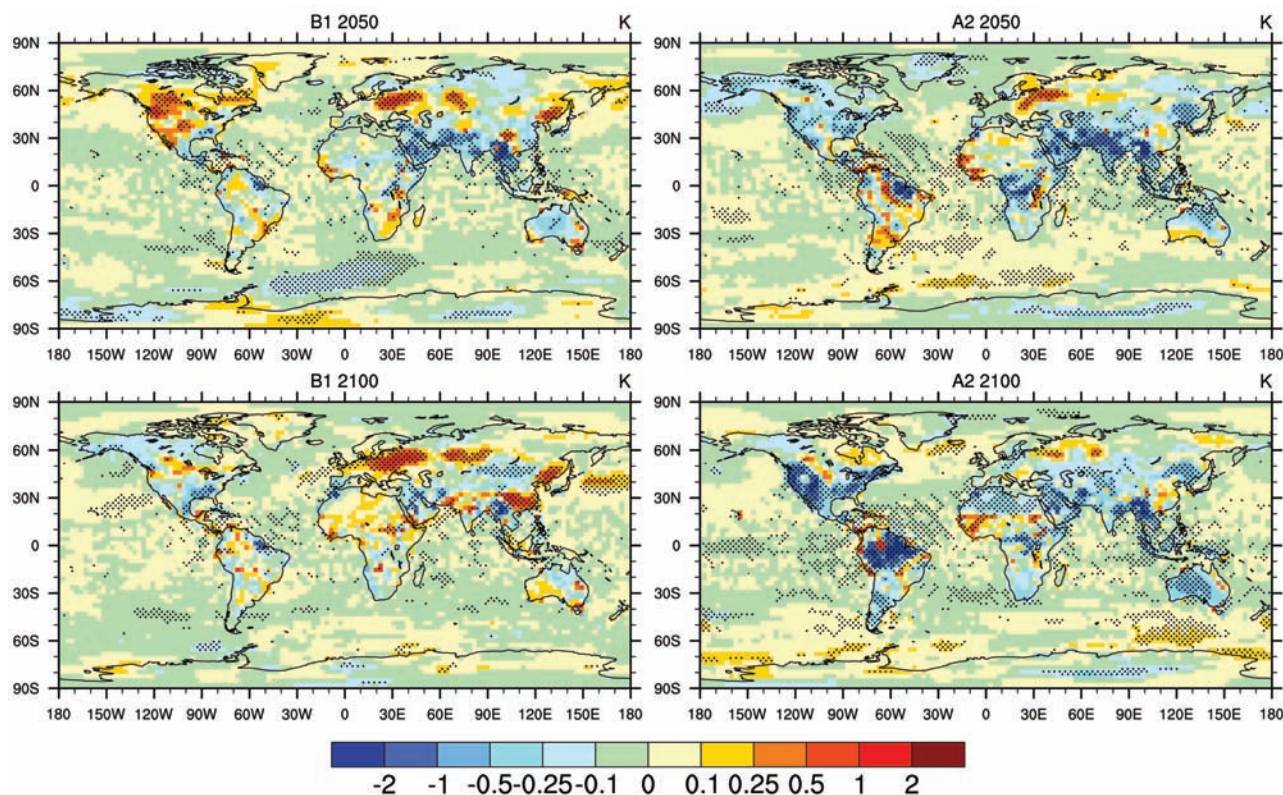


**Fig. 3.** Changes in the annual average diurnal temperature range due to land-cover change in each of the scenarios. Values were calculated by subtracting the greenhouse gas-only forcing scenarios from a simulation including land-cover and greenhouse gas forcings. Shaded grid cells are significant at the 0.05 confidence level.

In higher-latitude areas, particularly in the Northern Hemisphere, there are significant temperature changes that do not appear to be directly related to land-cover change. Although statistically significant, these changes are relatively small as compared to the projected atmospheric forcing changes. For example, in western Russia there is reforestation in both scenarios, which should lead to warming. However, although the additional land-cover changes have the expected impact on net radiation, the B1 and A2 scenarios show strongly opposing temperature signals in December, January, and February (DJF). These results appear to be closely linked to changes in regional precipitation and may be the result of teleconnections, either linked to the Asian Monsoon circulation or indirect effects from temperature changes over the tropical Pacific and North Atlantic Oceans.

Results from this study suggest that the choices humans make about future land use could have a significant impact on regional and seasonal climates. Some of these effects are the result of direct impacts of land-cover change on local moisture and energy balances. Other impacts appear to be related to significant indirect climate effects through teleconnection processes. The A2 land-cover scenario shows that tropical rainforest conversion will likely lead to a weakening of the Hadley circulation over much of the world and to significant changes in the Asian Monsoon circulation. Especially in the A2 2050 scenario, the interplay between Asian and African land-cover change affects the Asian Monsoon circulation. The Indian Ocean experiences a significant reduction in surface pressure, resulting in increased cloud cover and precipitation and warmer surface temperatures, and these effects extend over most of the Indian subcontinent.

We conclude that the inclusion of land-cover forcing, thereby accounting for a number of additional anthropogenic climate impacts, will improve the quality of regional climate assessments for IPCC SRES scenarios. Although land-cover effects are regional and tend to offset with respect to global average temperatures, they can significantly alter regional climate outcomes associated with global warming. Beyond local impacts, tropical land-cover change can potentially affect extratropical climates and nearby ocean conditions through atmospheric teleconnections. In this respect, our fully coupled experiments differ from previous fixed ocean temperature studies (12, 13, 15). Further study is needed to determine the exact nature of these responses. Overall, the results demonstrate the importance of including land-cover change in forcing scenarios for future climate change studies.

References and Notes

1. J. J. Houghton et al., Eds., *Climate Change 2000: The Scientific Basis* (IPCC Working Group I, Cambridge Univ. Press, Cambridge, 2001).

2. P. Kabat et al., *Vegetation, Water, Humans and the Climate Change: A New Perspective on an Interactive System* (Springer, Heidelberg, Germany, 2002).  
 3. W. Steffen et al., *Global Change and the Earth System: A Planet Under Pressure* (Springer-Verlag, New York, 2004).  
 4. R. A. Betts, *Atmos. Sci. Lett.* **2**, 39 (2001).  
 5. L. R. Bounoua, R. DeFries, G. J. Collatz, P. Sellers, H. Khan, *Clim. Change* **52**, 29 (2002).  
 6. T. N. Chase, R. A. Peilke Sr., T. G. F. Kittel, R. R. Nemani, S. W. Running, *Clim. Dyn.* **16**, 93 (2000).  
 7. J. J. Feddema et al., *Clim. Dyn.* **25**, 581 (2005).  
 8. J. Hansen et al., *Proc. Natl. Acad. Sci. U.S.A.* **95**, 12753 (1998).  
 9. H. D. Matthews, A. J. Weaver, K. J. Meissner, N. P. Gillett, M. Eby, *Clim. Dyn.* **22**, 461 (2004).  
 10. M. H. Costa, J. A. Foley, *J. Clim.* **13**, 18 (2000).  
 11. N. Gedney, P. J. Valdes, *Geophys. Res. Lett.* **27**, 3053 (2000).  
 12. K. McGuffie, A. Henderson-Sellers, H. Zhang, T. B. Durbidge, A. J. Pitman, *Global Planet. Change* **10**, 97 (1995).  
 13. R. S. DeFries, L. Bounoua, G. J. Collatz, *Global Change Biol.* **8**, 438 (2002).  
 14. S. Sitch et al., *Global Biogeochem. Cycles* **19**, GB2013 (2004).  
 15. R. Avissar, D. Werth, *J. Hydrometeorol.* **6**, 134 (2005).  
 16. R. A. Pielke Sr. et al., *Philos. Trans. R. Soc. London Ser. A* **360**, 1705 (2002).  
 17. G. Krinner et al., *Global Biogeochem. Cycles* **19**, GB1015 (2005).  
 18. P. K. Snyder, C. Delire, J. A. Foley, *Clim. Dyn.* **23**, 279 (2004).  
 19. G. B. Bonan, D. Pollard, S. L. Thompson, *Nature* **359**, 716 (1992).  
 20. G. A. Meehl et al., *Science* **307**, 1769 (2005).  
 21. W. M. Washington et al., *Clim. Dyn.* **16**, 755 (2000).  
 22. N. Nakićenović et al., *Special Report on Emissions Scenarios* (Cambridge Univ. Press, Cambridge, 2000).  
 23. J. Alcamo, R. Leemans, E. Kreileman, Eds., *Global Change Scenarios of the 21st Century. Results from the IMAGE 2.1 Model* (Pergamon Elsevier Science, London, 1998).  
 24. IMAGE 2.2 CD release and documentation (Rijks Instituut voor Volksgezondheid en Milieu, Bilthoven, Netherlands, 2002). The IMAGE 2.2 implementation of the SRES scenarios: A Comprehensive Analysis of Emissions, Climate Change and Impacts in the 21st Century (see www.rivm.nl/image/index.html for further information).  
 25. Materials and methods are available as supporting material on Science Online.  
 26. T. R. Karl, R. W. Knight, *Bull. Am. Meteorol. Soc.* **78**, 1107 (1997).  
 27. M. P. Hoerling, J. W. Hurrell, T. Xu, G. T. Bates, A. S. Phillips, *Clim. Dyn.* **23**, 391 (2004).  
 28. G. B. Bonan, *Ecol. Appl.* **9**, 1305 (1999).  
 29. G. B. Bonan, *J. Clim.* **14**, 2430 (2001).  
 30. We acknowledge the large number of scientists who have assisted in the development of the models and tools used to create the simulations used in this study. Special thanks to A. Middleton, T. Bettge, and G. Strand for their assistance in running the model and assistance with data processing and to R. Leemans for providing the SRES data. This research was supported by the Office of Science (Biological and Environmental Research Program), U.S. Department of Energy, under Cooperative Agreement No. DE-FC02-97ER62402; NSF (grant numbers ATM-0107404 and ATM-0413540); the National Center for Atmospheric Research Weather and Climate Impact Assessment Science Initiative supported by NSF; and the Center for Research, University of Kansas, Lawrence, KS.

Supporting Online Material

www.sciencemag.org/cgi/content/full/310/5754/1674/DC1

Materials and Methods

Figs. S1 and S2

References

29 July 2005; accepted 25 October 2005  
 10.1126/science.1118160

# Equivalent Effects of Snake PLA2 Neurotoxins and Lysophospholipid-Fatty Acid Mixtures

Michela Rigoni,<sup>1</sup> Paola Caccin,<sup>1</sup> Steve Gschmeissner,<sup>2</sup> Grielof Koster,<sup>3</sup> Anthony D. Postle,<sup>3</sup> Ornella Rossetto,<sup>1</sup> Giampietro Schiavo,<sup>2</sup> Cesare Montecucco<sup>1\*</sup>

Snake presynaptic phospholipase A2 neurotoxins (SPANs) paralyze the neuromuscular junction (NMJ). Upon intoxication, the NMJ enlarges and has a reduced content of synaptic vesicles, and primary neuronal cultures show synaptic swelling with surface exposure of the luminal domain of the synaptic vesicle protein synaptotagmin I. Concomitantly, these neurotoxins induce exocytosis of neurotransmitters. We found that an equimolar mixture of lysophospholipids and fatty acids closely mimics all of the biological effects of SPANs. These results draw attention to the possible role of local lipid changes in synaptic vesicle release and provide new tools for the study of exocytosis.

SPANs are major protein components of the venom of many snakes (1–3). They block the NMJ in a characteristic way (3–7). The phospholipase A2 (PLA2) activity varies greatly

among different SPANs, and its involvement in the NMJ block is still debated (3, 8, 9). There is only a partial correlation between PLA2 activity and neurotoxicity among SPANs and no overlap of surface residues required for neurotoxicity with those essential for PLA2 activity (8, 10). Here, we compared the effects of SPANs on the mouse NMJ hemidiaphragm preparation and on neurons in culture with those of their hydrolysis products: lysophospholipids (LysoPL) and fatty acids (FAs). To conclusively

<sup>1</sup>Department of Biomedical Sciences and Consiglio Nazionale Ricerche Institute of Neuroscience, University of Padova, Italy. <sup>2</sup>Cancer Research UK, London Research Institute, London, UK. <sup>3</sup>School of Medicine, University of Southampton, UK.

\*To whom correspondence should be addressed. E-mail: cesare.montecucco@unipd.it